

Metal carbonyl photochemistry in organic solvents: femtosecond transient absorption and preliminary resonance Raman spectroscopy

Alan G. Joly and Keith A. Nelson

Department of Chemistry, Massachusetts Institute of Technology, Cambridge, MA 02139, USA

Received 11 June 1990

Solvent effects in elementary chemical reactions are studied using femtosecond transient absorption spectroscopy. Photodissociation of $M(\text{CO})_6$ ($M = \text{Cr}, \text{Mo}, \text{or } \text{W}$) is examined in a variety of linear chain alcohols to ascertain the role of the solvent on the initial CO dissociation event. Resonance Raman experiments are also used to obtain more information about the reaction coordinate for CO dissociation. No significant solvent effects are seen on the short time (~ 350 fs) transient absorption signal assigned to CO dissociation; however, effects are seen on an intermediate timescale attributed to differences in solvent complexation dynamics. Subsequent vibrational cooling of the nascent $\text{Cr}(\text{CO})_5(\text{SOLVENT})$ complex is observed consistent with earlier results.

1. Introduction

Recently there has been much interest in probing the dynamics and potential energy surfaces of chemically reactive species [1,2]. For small molecules in the gas phase, unimolecular dissociation dynamics may be determined uniquely by the structure of the potential energy surface along which reaction occurs. Real-time observations of such reactions have recently become possible, and the dynamics measured can provide detailed information about reactive potential energy surfaces [3,4]. In condensed phases, interactions between the reacting species and its environment cause dissipation of momentum along the reaction coordinate, barrier recrossing, and other events which destroy the one-to-one correspondence between reactive potential energy surface (PES) and reaction dynamics. A microscopic understanding of condensed phase chemical reactions therefore requires independent determination of both chemical reaction dynamics and reactive potential energy surface. Given these, critical analysis of lattice or solvent ("bath") effects on reaction dynamics, yield, etc. can be undertaken. Such an analysis poses additional requirements for information about the molecular dynamics of the bath itself, including the strengths of

intermolecular forces between bath molecules and between bath and reacting species.

We have taken several initial steps toward understanding condensed phase chemical reactions of simple organometallic species. To put the goals of our work in perspective, it is useful to outline the following protocol even though we are far from executing all the steps.

(1) Reaction dynamics can be determined through femtosecond time-resolved spectroscopic measurements such as those discussed below.

(2) Potential energy surfaces must be inferred from a variety of spectroscopic methods, including femtosecond time-resolved spectroscopy, resonance Raman spectroscopy, absorption and fluorescence measurements, etc., as well as from theoretical calculations. Since detailed features of intramolecular potential energy surfaces are likely to be washed out by the intermolecular interactions and inhomogeneity of the bath, highly accurate PES determination should not be necessary.

(3) Molecular dynamics and intermolecular interactions of the nonreactive bath must be modeled.

(4) Given (2) and (3), simulations of chemical reaction dynamics in the bath can be carried out. The

simulation results can be compared to experimental data (1).

The results of the comparison can be used to refine the assumptions and procedures used in (4). This is ultimately the critical step which we hope to reach. Very different models have been proposed for treating unimolecular photodissociation in a liquid, in which at least one of the photofragments must “break out” of the immediate solvent environment to avoid rapid recombination. Starting points suggested for the treatment range from a “rigid cage” picture [5] to one in which the solvent is envisioned as highly compliant and always in an equilibrium configuration around the dissociating species (in which case a potential of mean force can be used to describe the intermolecular interactions) [6–8]. The conditions under which these or other starting points are reasonable, and the manner in which refinements can be made, comprise in our view one of the central problems in condensed phase physical chemistry. The problem is especially challenging because in general the time scales for bond breakage, photofragment disruption of the solvent “cage”, and nonreactive bath dynamics cannot be separated.

Advances in both time and frequency-domain spectroscopies have raised hopes for experimental determination of potential energy surfaces and chemical reaction dynamics. Time-domain experiments can be carried out with pulses whose durations are short compared to the time required for any significant nuclear motion in the direction of chemical change. Phase-coherent nuclear motion (i.e. phase-coherent wavepacket propagation) in an electronic excited state is initiated upon absorption of an ultrashort pulse, and can be monitored through measurement of absorption of other, variably delayed pulses. As illustrated in fig. 1, photoexcitation with an ultrashort pulse into a bound potential (S_1) results in excited molecules whose vibrational oscillations are in phase. Variably delayed probe pulses then encounter the excited molecules at various stages of oscillation, permitting spectroscopic characterization of vibrationally distorted species as well as measurement of excited-state vibrational frequencies and dephasing rates [9–11]. Similarly, absorption into an unbound potential (S_3) initiates synchronized or phase-coherent motion which is not oscillatory but rather monotonic, e.g. stretching of a bond distance

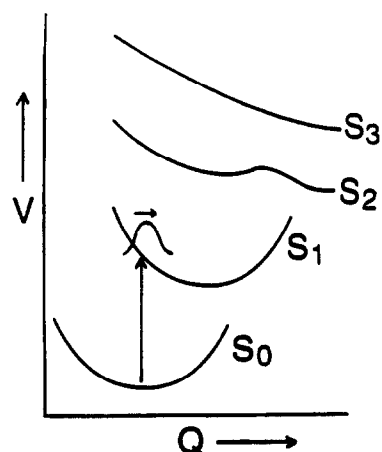


Fig. 1. Schematic illustration of electronic potential energy surfaces as a function of the vibrational coordinate Q . Optical absorption into S_1 leads to coherent oscillations about the excited state potential minimum. Absorption into S_2 or S_3 leads to coherent wavepacket propagation from the excited state to the dissociated product.

until dissociation occurs. This process can also be probed through measurement of transition absorption spectra, provided the excitation and probe pulse durations are short relative to the dissociation time [3,4]. This provides a good measure of the reaction dynamics and, depending upon what is known about the final state into which absorption (or stimulated emission) occurs, may also yield information about the reactive potential energy surface and about environmental effects on the reacting species.

A set of prototypical liquid-state photochemical reactions is offered by the metal carbonyls $M(\text{CO})_6$ where $M = \text{Cr}, \text{Mo},$ or W and $M_2(\text{CO})_{10}$ where $M = \text{Mn}$ or Re . These species are of substantial chemical interest, but are also simple enough to be amenable to spectroscopic investigation and theoretical calculations. We have presented preliminary femto-second time-resolved transient absorption spectra from both families [12,13], and we will concentrate here on the first which has been the subject of a number of recent time-resolved electronic and vibrational spectroscopic investigations [21,14–17]. In the gas phase, absorption of an ultraviolet photon yields a variety of fragments [14,18,19], $\text{Cr}(\text{CO})_n$ where $n = 0–5$. In solution, only a single CO dissociates, presumably because energy transfer to the surrounding bath dissipates excess $\text{Cr}(\text{CO})_5$ internal energy

and thereby quenches further reaction. Previously we determined that the CO dissociation was complete within 350 fs [12]. After dissociation, a nearby solvent molecule coordinates to the naked site, forming the species $\text{Cr}(\text{CO})_5\text{S}$ ($\text{S}=\text{solvent}$) which is stable onto at least the nanosecond time scale. Solvent complexation produces a new visible absorption whose maximum is known to reflect the strength of the Cr–S bond [20–22]. Recently, Simon and Xie [15] as well as Joly and Nelson [12] have measured the rise time of the visible $\text{Cr}(\text{CO})_5(\text{MeOH})$ absorption to be approximately 2.5 ps. Both groups have attributed this time to the bonding of the solvent to the bare coordination site. We note that Spears and co-workers [16] have performed picosecond ultraviolet pump and infrared probe experiments whose results suggested that the “naked” $\text{Cr}(\text{CO})_5$ is long-lived (~ 100 ps) and exists in two different forms, the C_{4v} symmetry square pyramidal and the D_{3h} symmetry trigonal bipyramid, both of which may complex with the solvent. Visible absorption measurements using polarized light have inferred two distinct intermediates in low-temperature matrices [23]. The implications of these observations for the room temperature liquid phase visible absorption spectrum is not known, and to date no evidence of more than one $\text{Cr}(\text{CO})_5$ conformer has been seen in the solution phase electronic spectrum. Very recent measurements of transient Raman spectra [24] appear to support the conclusion that solvent coordination occurs within several picoseconds.

We present new femtosecond transient absorption data on all three metal carbonyls, $\text{M}(\text{CO})_6$ with $\text{M}=\text{Cr}, \text{Mo}, \text{W}$, in several organic solvents. The results in each case indicate the dynamics of the initial ligand ejection event as well as the time scales of subsequent solvent complexation and relaxation. Although transient excited-state–excited-state absorption spectra of dissociating $\text{M}(\text{CO})_6$ species will not allow us to elucidate in detail the reactive potential energy surfaces, we can hope to address two basic questions that have raised concern. The reaction dynamics should indicate (1) whether reaction occurs in the initially excited singlet state, or whether the nearby triplet level plays an essential role; and (2) whether the singlet excited state, if reactive, is unbound or weakly bound (as in level S_3 or S_2 respectively of fig. 1).

Considerable information about the structures of excited-state potential energy surfaces can be obtained through resonance Raman spectroscopy. We present preliminary resonance Raman spectra which suggest a possible reaction path in metal hexacarbonyls. We also present preliminary data from dimanganese decacarbonyl, $\text{Mn}_2(\text{CO})_{10}$, which offer some insight into the metal–metal bond photocleavage reaction that can occur upon absorption.

2. Experimental

The femtosecond laser system used has been described previously [25]. Briefly, a cw modelocked Nd:YAG laser synchronously pumps a femtosecond dye laser operating with rhodamine 590 as the gain medium and DODCl as the absorber. The output of this laser consists of 65 fs pulses at 82 MHz, centered at 615 nm with 45 mW average power. These pulses are amplified in a three stage amplifier which is longitudinally pumped by the frequency doubled output of a seeded Nd:YAG regenerative amplifier. After compression using a SF_6 prism pair, the resulting pulses are 55 fs in duration with a pulse energy of 10 μJ and an 800 Hz repetition rate.

Seventy percent of this output is frequency doubled in a 1 mm KDP crystal to yield the 308 nm, 90 fs, 400 nJ pump pulses. The remaining 30 percent is focussed into a 2 mm cell of D_2O to produce a white light continuum pulse spanning the spectral range of 400–900 nm. A 10 nm interference filter is used to select the desired probe wavelength. The probe pulse is variably delayed along a stepping-motorized delay line and then overlapping spatially with the pump pulse inside the sample. The polarizations of the pump and probe beams are adjusted to be 55 degrees apart to eliminate the effects of molecular rotation on the signal. The intensities of the probe before and after the sample (I_0 and I_t respectively) are measured and the quantity $(I_t - I_0)/I_t$ is determined. Typical values of $(I_t - I_0)/I_t$ are between 2 and 10 percent. Different interference filters separated by 20 nm were used to select different probe wavelengths, and broadband transient absorption spectra were constructed from all the data obtained. Cross correlations between ultraviolet and probe pulses indicate an instrument response of approximately 100 fs which

is consistent with the fastest rise times seen in the data. Control experiments on trans-stilbene, which undergoes no photochemical change on sub-picosecond times scales, also show 100 fs rise times.

Additional control experiments were conducted on high-purity solvents only, without the organometallic solute present. There is appreciable transient absorption signal from most solvents, presumably due to electronic excited states produced by two-photon absorption of the ultraviolet excitation pulse. This signal varies in timescale and form in different solvents but in all cases the transient absorption strength is greatest at $t \approx 0$ and decays rapidly to a lower level, which in some cases persists for longer times. The pure solvent absorption strength at $t \approx 0$ at any probe wavelength reported in this work is at least a factor of 4 smaller (and often a factor of ten smaller) than any signal obtained with $M(\text{CO})_6$ present. At longer times, the signal due to solvent is even weaker by comparison. Solvent transient absorption was not considered in our data analysis.

The samples are saturated (10^{-3} M) solutions in high-purity solvents, flowed through quartz flow cells. To minimize optical damage of the walls of the flow cell, the cell is translated slightly along a motorized translation stage after each laser shot. Even with this precaution taken, the optical quality of the flow cell can undergo gradual deterioration during an experiment. The amount of probe light scattered by the cell can therefore increase gradually. To eliminate spurious effects on the data, measurements at each point on the probe pulse delay line are taken with and without the pump pulse present and the scattered light intensity is subtracted. In addition, the entire delay line is scanned several times in an experiment.

Raman experiments are performed using a cw Ar⁺ or Kr⁺ ion laser operating on the 514 or 351 nm line, respectively. The backscattered radiation is passed through a polarization scrambler and focussed into a Spex $\frac{1}{2}$ meter scanning double monochromator and detected using a photon counting system. The sample is a saturated solution of $M(\text{CO})_6$ in methanol flowed through a 1 mm diameter jet.

When performing experiments on photochemically active samples, it is important to produce as few photoproducts as possible. It is generally acceptable to keep the photoalteration parameter F defined below [26,27] under 0.1.

$$F = \frac{2303}{N_a} \left(\frac{P}{Dv} \right) \epsilon \phi, \quad (1)$$

where N_a is Avogadro's number, ϵ the molar decadic extinction coefficient, ϕ the photochemical quantum yield, D the largest dimension of the beam, P the photon flux, and v the flow velocity. For $\text{Cr}(\text{CO})_6$ at the peak of the ligand field transition ($\epsilon_{\text{max}} \approx 3000 \text{ l M}^{-1} \text{ cm}^{-1}$) and assuming a flow of 0.5 m/s, $F = 0.05$ when 3 mW average cw power is used. The 351 nm excitation light is not at the peak but is near resonance ($\epsilon_{351} \approx 300 \text{ l M}^{-1} \text{ cm}^{-1}$). In order to keep the photoalteration ratio below 10 percent, very low (<25 mW) powers were used when near resonance.

3. Results and discussion

3.1. Transient absorption spectra from $M(\text{CO})_6$ in methanol and hexane solvents

Ultraviolet pulses at 308 nm excite predominantly the ${}^1A_{1g} \rightarrow {}^1T_{1g}$ ligand field transition in $\text{Cr}(\text{CO})_6$ [28]. This excited state is known to lead to CO ligand loss within 3 ps [12,15]. Fig. 2 shows transient absorption data of $\text{Cr}(\text{CO})_6$ in methanol taken with

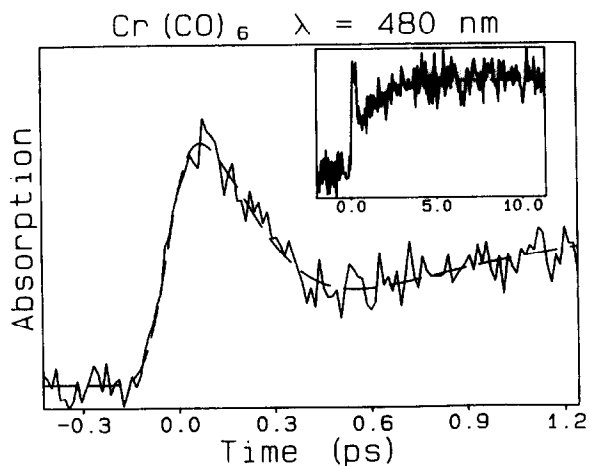


Fig. 2. Transient absorption data of $\text{Cr}(\text{CO})_6$ in methanol using probe pulses at $\lambda = 480$ nm. The initial (350 fs) nonexponential decay is a signature of coherent wavepacket propagation on a repulsive surface. The scan indicates that CO dissociation is complete in ~ 350 fs after which solvent complexation occurs in ~ 3 ps.

308 nm pump and 480 nm probe pulses. The probe wavelength corresponds to the absorption maximum of the solvent complexed species $\text{Cr}(\text{CO})_5(\text{MeOH})$. The data show three distinct regions: a pulse-duration limited rise, a rapid (< 500 fs) nonexponential decay, and a slower, 1.6 ps exponential rise. The slow rise is similar to that reported earlier by Simon and Xie [15] who attribute it to the complexation of the solvent. The pulse-duration limited rise represents population of the initially excited ligand field state. The rapid nonexponential decay represents coherent wavepacket propagation on a symmetric, repulsive potential. The excited-state-excited-state absorption spectrum of the $^*\text{Cr}(\text{CO})_6$ species shifts during dissociation, reflecting the degree to which the Cr-CO bond is stretched. The data indicate that the dissociation is complete within 350 fs.

We have obtained the time-dependent excited-state absorption spectra of all three $\text{M}(\text{CO})_6$ species. Fig. 3 depicts the spectral changes of $\text{W}(\text{CO})_6$ for the first 5.7 ps after absorption. Data from $\text{Cr}(\text{CO})_6$ and $\text{Mo}(\text{CO})_6$ are almost identical in form, as shown by figs. 4 and 5. Data from $\text{W}(\text{CO})_6$ have higher signal/

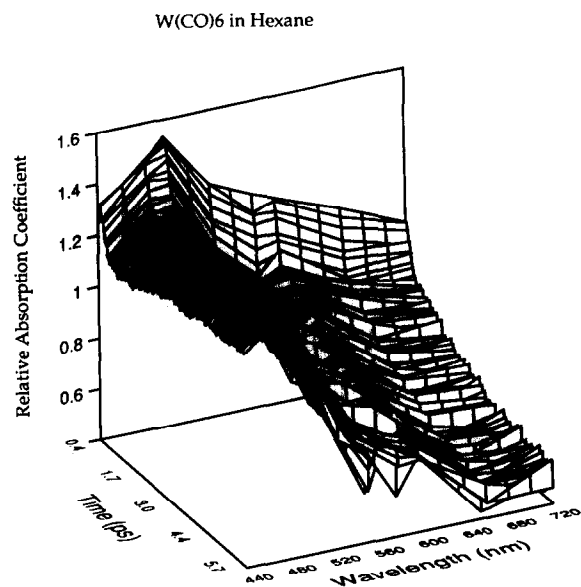


Fig. 3. Broadband visible absorption spectra for $\text{W}(\text{CO})_6$ in hexane. The excited-state-excited-state absorption spectrum is peaked at 500 nm and decays in 350 fs. Subsequent solvent complexation leads to a gradual rise between 440 and 520 nm indicating formation of the product $\text{W}(\text{CO})_5(\text{hexane})$.

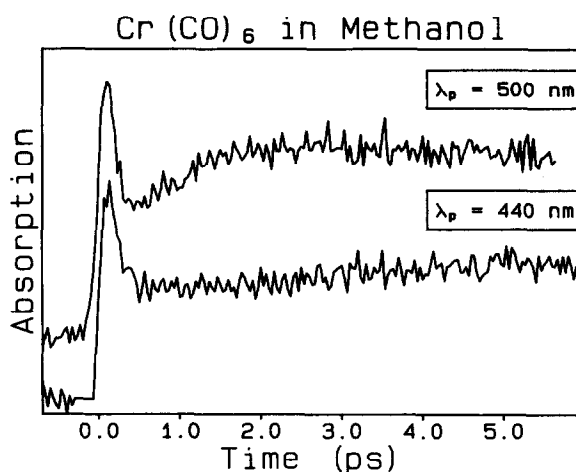


Fig. 4. Transient absorption data for $\text{Cr}(\text{CO})_6$ in methanol for probe wavelengths of $\lambda = 500$ nm (top) and $\lambda = 440$ nm (bottom). The form and timescale of the signal are similar to those from $\text{W}(\text{CO})_6$.

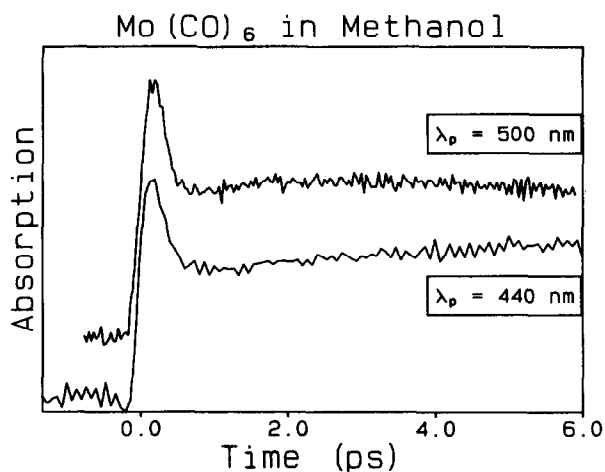


Fig. 5. Transient absorption data for $\text{Mo}(\text{CO})_6$ in methanol shows the same qualitative features as data from $\text{Cr}(\text{CO})_6$ and $\text{W}(\text{CO})_6$ at the same probe wavelengths.

noise ratios due to an increase in $^1\text{A}_{1g} \rightarrow ^1\text{T}_{1g}$ absorption strength. Relative absorption measurements at any one wavelength are precise to ± 5 percent or better, as indicated by the signal/noise level in the individual sweep. Some regions of broadband spectra such as those in fig. 3 have been interpolated; however, we believe that our measurements of relative absorption strengths at different wavelengths are precise to ± 10

percent. Fig. 3 indicates that the excited-state absorption spectrum of $W(CO)_6$ is peaked at 500 nm and tails to the blue. During the first 500 fs, as CO loss occurs, the absorption strength decays sharply and blue shifts slightly. During the next several picoseconds the spectrum shows a more gradual increase in absorption between 440 and 500 nm. This was interpreted by Simon and Xie [15] and later by us [12] as a signature of solvent complexation, i.e. formation of the $W(CO)_5(\text{Hexane})$ species. Further spectral evolution over a total of 70 ps after photoexcitation is shown in fig. 6. Within about 50 ps the absorption maximum has shifted from 500 nm to 480 nm which we [12] and others [17] have attributed to vibrational relaxation of the solvent complexed species. After 70 ps, the absorption maximum is centered at approximately 480 nm which we believe represents the vibrationally cooled product $W(CO)_5(\text{MeOH})$. No further spectral evolution is seen on picosecond time scales.

Transient absorption data from $Cr(CO)_6$ and $Mo(CO)_6$ over temporal ranges of about 60 picoseconds are shown in figs. 7 and 8. In each species, time-

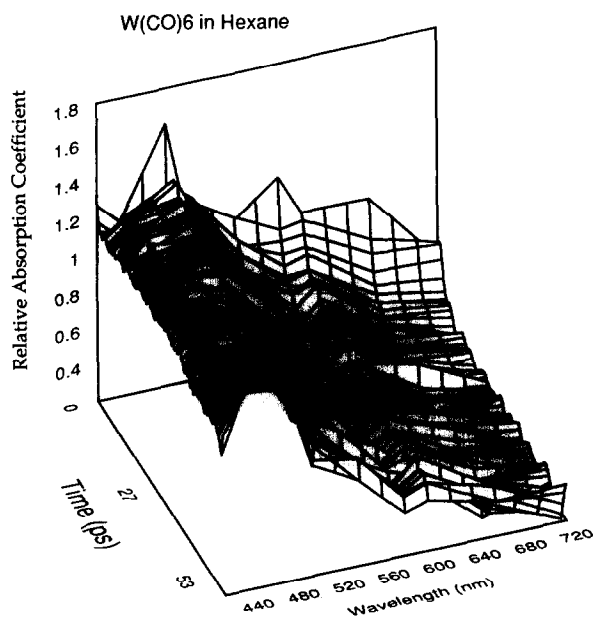


Fig. 6. Spectral evolution of $W(CO)_5(\text{hexane})$ for 70 ps after excitation. The absorption maximum of $W(CO)_5(\text{hexane})$ shifts from 500 nm to 480 nm in ~ 50 ps, indicating that vibrational relaxation of the solvated species occurs on this timescale.

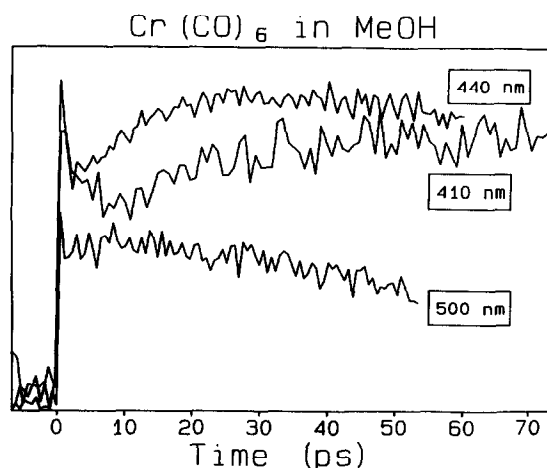


Fig. 7. Spectral evolution of $Cr(CO)_5(\text{MeOH})$ for 70 ps. The three sweeps show that the absorption spectrum gradually blue shifts. This is attributed to vibrational relaxation which occurs in approximately 50 ps, as in $W(CO)_5(\text{MeOH})$.

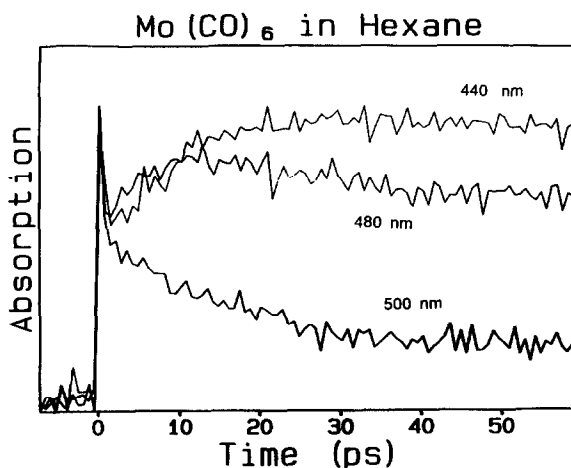


Fig. 8. Spectral evolution of $Mo(CO)_5(\text{MeOH})$ for 60 ps shows similar features to the W and Cr analogs. The vibrational relaxation dynamics of all three solvent complexed species are nearly identical.

dependent spectral evolution indicates three distinct time scales. We associate the first 500 fs with CO dissociation, the 0.5–5 ps interval with solvent complexation, and the 5–50 ps regime with vibrational relaxation of the $M(CO)_5S$ species. This final assignment of the gradually blue-shifting spectrum is consistent with earlier results on iodine vibrational relaxation in solution [29].

We note that there are several issues which are not clearly resolved by transient visible absorption spectra. First, the time scale for electronic relaxation is not completely clear. We have assumed that the bare $M(\text{CO})_5$ species is formed in its ground electronic state since we see no clear spectral signature of $M(\text{CO})_5$ electronic relaxation. Ab initio calculations [30] have suggested that the bare pentacarbonyl may be produced in its first excited electronic state. Second, the presence of two different conformers (D_{3h} and C_{4v}) of the bare $M(\text{CO})_5$ species as concluded from transient vibrational spectra by Spears and co-workers [16] cannot be resolved from the electronic spectra. As indicated earlier, we believe that the kinetics of transient electronic absorption data [12,15] and recent transient Raman data [24] indicate solvent complexation of the bare pentacarbonyl species within 5 ps.

Some questions about the nature of the photodissociative state can be addressed by our results from the three compounds. In particular, the role of the triplet ligand field state has long been uncertain. The absorption spectrum of $\text{W}(\text{CO})_6$ displays a weak shoulder at 375 nm which has been attributed to the $^1A_{1g} \rightarrow ^3T_{1g}$ transition [31]. Nasielski and Colas [32] found that the quantum yield for dissociation in $\text{W}(\text{CO})_6$ is independent of wavelength implying that photochemistry occurs from the triplet state. Since the spin-orbit coupling is much stronger in $\text{W}(\text{CO})_6$ than in $\text{Cr}(\text{CO})_6$, involvement of the triplet state should influence the form or decay time of the initial transient in the 0–500 fs range. Fig. 9 shows the results of transient absorption measurements in $\text{Cr}(\text{CO})_6$, $\text{Mo}(\text{CO})_6$, and $\text{W}(\text{CO})_6$ at 480 nm. The short-time signal in all three appears identical. There are two plausible explanations for this behavior. Either dissociation from the initially excited singlet state occurs before any significant intersystem crossing into the triplet state can take place, or else intersystem crossing is extremely efficient and occurs within 100 fs in all three species. Such rapid intersystem crossing rates cannot be ruled out by our data, but we feel they are extremely unlikely. We conclude that the reaction proceeds directly from the initially excited state with no intersystem crossing necessary.

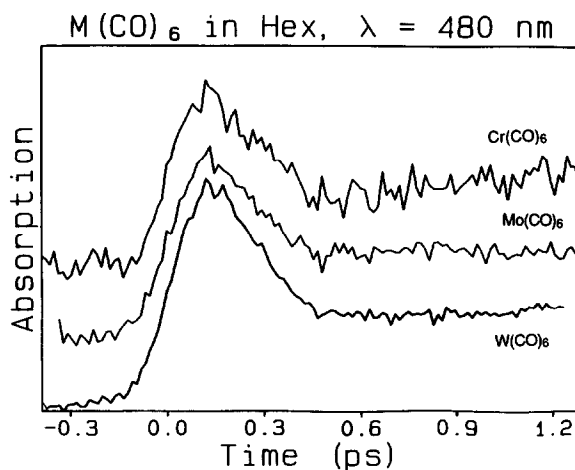


Fig. 9. Transient absorption data from $\text{Cr}(\text{CO})_6$, $\text{Mo}(\text{CO})_6$, and $\text{W}(\text{CO})_6$ in hexane. The short time transient is identical in form and timescale in all three. This indicates that intersystem crossing, whose rate should increase considerably with the metal atomic weight, is not involved in the short time dynamics. The triplet state apparently does not play a significant role in the dissociation process.

3.2. Transient absorption spectra from other solvents

We have investigated the metal carbonyls in several solvents in order to explore the role of the solvent on each of the three photophysical processes – ligand ejection, solvent complexation, and vibrational relaxation. The solvents used for our studies are hexane, methanol, ethanol, 1-propanol, 1-pentanol, 1-octanol, and ethylene glycol. The widely varying molecular sizes and viscosities of these solvents permit evaluation of whether these properties have effects on the initial dissociation and ensuing complexation dynamics.

We have concentrated on the probe wavelength region from 440 to 500 nm since transient absorption spectra in this regime are sensitive to all three processes. Fig. 10 depicts transient absorption data from $\text{Cr}(\text{CO})_6$ in methanol, hexane, and ethylene glycol. To within our signal/noise, there is no appreciable difference in the short time (0–500 fs) decay even in the viscous solvent ethylene glycol. In fact, the short time signal is essentially identical in all the solvents used. This implies that the initial dissociation of CO is influenced very little by solvent forces. It appears that the short time dynamics are determined almost

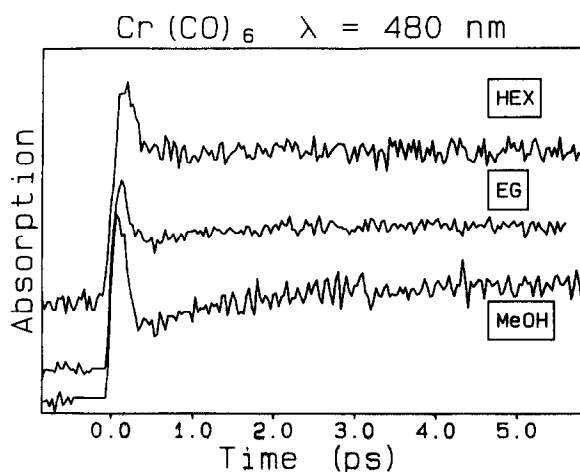


Fig. 10. Transient absorption data for $\text{Cr}(\text{CO})_6$ in methanol, hexane and ethylene glycol. In MeOH and ethylene glycol (EG), the data show a gradual rise indicative of solvent complexation. In hexane, no such feature is apparent. This is due to the small spectral effects of complexation of $\text{Cr}(\text{CO})_5$ to an alkyl moiety. Complexation to the hydroxyl moiety of alcoholic solvents has larger effects on the absorption spectrum.

solely by the intramolecular PES. Clearly, the ejected ligand must eventually perturb the surrounding bath substantially, and will either escape entirely from its parent or undergo geminate recombination. We note that the high quantum yield of 0.7 for photodissociation [33] implies that most of the dissociated ligands escape the solvent cage. Our data indicate that interactions with the solvent occur after the ligand is no longer strongly interacting with the parent compound whose spectral behavior is probed.

Fig. 10 does show differences in the 1–5 ps regime, lending support to the association of this time scale with solvent complexation. In methanol and ethylene glycol there is a gradual rise in absorption while in hexane no such feature is present. At present we have not unambiguously observed a solvent rise for $\text{Cr}(\text{CO})_6$ in hexane at any wavelength. However, we have observed such a rise in $\text{Mo}(\text{CO})_6$ and $\text{W}(\text{CO})_6$ in hexane. It is probable that the changes in the $\text{Cr}(\text{CO})_5$ (hexane) absorption spectrum are not strong enough for us to detect, while in $\text{W}(\text{CO})_6$ and $\text{Mo}(\text{CO})_6$ the effect appears stronger. The gradual rise in fig. 10 has the same time constant (1.6 ± 0.2 ps assuming exponential reaction kinetics) for both methanol and ethylene glycol. Fig. 11 shows tran-

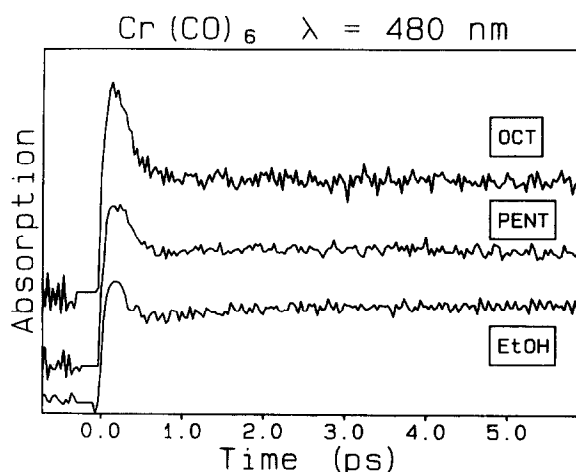


Fig. 11. Transient absorption data for $\text{Cr}(\text{CO})_6$ in ethanol, 1-pentanol, and 1-octanol. The gradual rise attributed to solvent complexation is visible in ethanol and pentanol. In octanol the predominance of alkyl complexation leads to minimal spectral change.

sient absorption data of $\text{Cr}(\text{CO})_6$ in ethanol, 1-pentanol, and 1-octanol. In ethanol, 1-propanol (not shown), and 1-pentanol the absorption rise time is identical but the signal strength decreases as the alcohol chain length increases. In octanol, the data are similar to those in hexane. Table 1 summarizes the results of transient absorption measurements in the 1–5 ps range for all three $\text{M}(\text{CO})_6$ compounds in various solvents using probe wavelengths at or near the absorption maximum of $\text{M}(\text{CO})_5\text{S}$. It is clear that solvent viscosity, dielectric constant, and molecular weight have no systematic effects on complexation dynamics on this time scale. The measurements are complicated somewhat by the fact that the transient absorption rise time for the solvent coordinated species is wavelength dependent. Measurements on the red edge of the absorption band show faster rise times than those measured on the blue edge in all metal carbonyls and solvents listed. This is an indication that the spectrum is blueshifting slightly on this timescale as well, making it difficult to assign a definitive complexation time.

Examination of the $\text{Cr}(\text{CO})_6$ data in figs. 10 and 11 shows that the dynamics of spectral evolution in the 1–5 ps regime do not depend on the solvent, but the extent of spectral change does. The results indicate that solvent complexation dynamics are essen-

Table 1
Rise time associated with solvent complexation

Solvent	Viscosity ^{a)}	Transient absorption rise time ^{b)}		
		Cr(CO) ₆ ^{c)}	Mo(CO) ₆ ^{d)}	W(CO) ₆ ^{d)}
Hexane	0.326	N/A ^{e)}		3.0
Methanol	0.597	1.6	3.0	2.3
Ethanol	1.2	1.6		
1-Propanol	2.3	1.6		
1-Pentanol	4.0	1.6		
1-Octanol	10.6 ^{f)}	N/A		
Ethylene glycol	19.9	1.6		

^{a)} Viscosities are in units of cp, at 20°C. ^{b)} Times are in picoseconds, $\pm 10\%$ uncertainties. ^{c)} Probe wavelength of 480 nm. ^{d)} Probe wavelength of 440 nm. ^{e)} No gradual rise in transient absorption was observed. ^{f)} Viscosity in cp at 15°C.

tially identical in all solvents, but the complexation of different solvents causes varying amounts of change in the absorption coefficients. The insensitivity of the dynamics with respect to solvent implies that solvent macroscopic properties such as viscosity and dielectric constant do not determine the complexation time. Instead this rise time indicates the time needed for any nearby solvent molecule to complex with the nascent Cr(CO)₅ species. The varying amounts of spectral change indicate that complexation to a hydroxyl moiety has far more effect on the absorption spectrum than complexation to an alkyl moiety. In alcohols, both the hydroxyl and alkyl moieties may complex with the naked species. As the alcohol chain length grows progressively longer, the probability that an OH end is near the vacant site diminishes. Thus the absorption signal in longer chain alcohols is statistically weighted toward coordination to the alkyl species. This explains the diminishing amount of change in signal as the alcohol chain length increases. In octanol, the initial fraction of OH-coordinated species is quite small and thus the signal resembles that from hexane.

Although in alcohols coordination to either hydroxyl or alkyl moieties may occur initially, the former is more stable thermodynamically. This is consistent with results of Xie and Simon [34] who show that alkyl coordinated species ultimately undergo rearrangement to form only the hydroxyl coordinated species. Rearrangement occurs on the 100–400 ps timescale depending on chain length [34]. Our results and theirs indicate that the initial local solvent structure undergoes little or no rearrangement before

complexation, resulting in a mixture of complexed species. The results also suggest that the initial solvent configuration does not determine which of the six CO's dissociates, but instead determines which part of the solvent complexes to the naked site.

The transient absorption results of this study and those done earlier provide a consistent picture of metal carbonyl photochemistry in simple organic solvents. In each M(CO)₆ compound, the initial photoejection of CO occurs within 500 fs and shows no significant influence of the solvent. Complexation of the resulting M(CO)₅ species with a solvent molecule occurs within the next several picoseconds. The M(CO)₅S species formed initially is controlled kinetically, with no obvious preference for the complex which is most stable thermodynamically. Vibrational relaxation of the initially hot M(CO)₅S species occurs on 50 ps time scales.

3.3. Resonance Raman spectra of Cr(CO)₆ and Mn₂(CO)₁₀

Although we know the time scale for initial CO photoejection rather well, we still know little about the reaction coordinate, including the intramolecular geometry changes accompanying ligand loss. One might expect substantial deformation of the parent complex along various vibrational coordinates, as has been demonstrated through resonance Raman spectroscopy [2] (and recently through femtosecond time-resolved measurements [4]) for methyl iodide in the gas phase. To address the question of the reaction coordinate, we have performed resonance Ra-

man (RR) experiments on $\text{Cr}(\text{CO})_6$ in methanol. In RR, as the frequency of the excitation light approaches an electronic resonance, there is enhancement in those vibrational modes which undergo distortion in the electronic excited state. Measurement of the enhancement of these modes as a function of excitation frequency [the resonance enhancement profile (REP)] may then yield information about the structure of the excited-state PES. Those vibrational modes which determine the dissociative coordinate will have large distortions in the excited state and undergo large enhancement. Identifying these modes gives important information about the reaction coordinate [35,36].

As discussed in the experimental section, resonance Raman spectra were collected with very low excitation laser intensities to minimize the extent of photodissociation. Due to the limited tuning range of our excitation source, we could only obtain spectra in the pre-resonant region. This does not allow us to carry out a complete study, but the results are suggestive and indicate that further work along these lines is called for.

$\text{Cr}(\text{CO})_6$ has 33 normal modes, two of which are totally symmetric. It is clear that the totally symmetric A_{1g} Cr–CO “breathing” mode is not the main part of the reaction coordinate as this displaces all six CO’s by the same amount. Therefore there must be participation of at least one asymmetric stretch. Due to symmetry considerations in the Franck–Condon (FC) factors, enhancement of asymmetric stretches is manifested by the appearance of even overtones in the Raman spectrum. There is one additional consideration due to the symmetry of the electronic transition. The ${}^1A_{1g} \rightarrow {}^1T_{1g}$ ligand field transition is formally symmetry forbidden, implying that the well-known Albrecht A-term [37] given by

$$\alpha_A \propto |M_{eg}^0|^2 \sum_{e,v} \frac{\langle j|v\rangle \langle v|i\rangle}{E_v - E_0 + i\Gamma_{ev}} \quad (2)$$

does not apply. Here, M_{eg} is the electronic transition moment between the ground state $|g\rangle$ and the excited state $|e\rangle$, i is the initial vibrational level, j the final vibrational level, and v is a vibrational level in the excited state, E_0 is the laser frequency, and E_{ev} and Γ_{ev} are the energy and dephasing rate of the $|ev\rangle$ state. The Albrecht B-term [37] is also for symmetry allowed transitions and does not apply here.

The first important term for symmetry forbidden electronic transitions may be written [38,39] as

$$\alpha \propto (A_{es}^a)^2 M_{gs} M_{sg} \sum_{e,v} \frac{\langle j|Q_a|v\rangle \langle v|Q_a|i\rangle}{E_0 - E_{ev} + i\Gamma_{ev}}, \quad (3)$$

where state $|s\rangle$ is symmetry allowed from $|g\rangle$ and couples to $|e\rangle$ through the vibronic mixing Hamiltonian, (A_{es}^a) , Q_a is a vibronic promoting mode through which absorption spectral intensity for the $|e\rangle$ state occurs, and M_{gs} is the electronic transition moment between $|g\rangle$ and the symmetry allowed state $|s\rangle$.

The FC factors for a mode that is not the vibronic mixing mode are identical to those in the A-term case. Resonance enhancement in such a mode will give rise to even overtones. The FC factors for a vibration that is the vibronic coupling mode vanish due to symmetry considerations for the fundamental transition, but for the 0→2 overtone are given by

$$\begin{aligned} \langle j_a|Q_a|v_a\rangle \langle v_a|Q_a|i_a\rangle &\propto \langle 2|Q_a|v_a\rangle \langle v_a|Q_a|0\rangle \\ &= \langle 3|v_a\rangle \langle v_a|1\rangle + \langle 1|v_a\rangle \langle v_a|1\rangle. \end{aligned} \quad (4)$$

The second term may give significant intensity to the 0→2 overtone of the promoting mode even if it is not the reaction coordinate, i.e. even if extensive motion along the mode does not occur in the excited state. In fact, on resonance with a forbidden transition, the 0→2 overtone of the vibronic mixing mode may undergo more enhancement than any other mode. Observations of vibronic overtones have been observed in the forbidden bands of benzene [39,40] and have been used to locate the $2\ {}^1A_g$ electronic state in butadiene [41]. Therefore only the observation of higher overtones (0→4, 0→6, etc.) can rigorously determine that a given Raman active asymmetric stretch is part of the reaction coordinate.

These considerations may be somewhat clearer physically in terms of the wavepacket description of the Raman-scattering cross section originally elucidated by Lee and Heller [35]. The cross section $\alpha_{i \rightarrow f}$ is given by

$$\alpha_{i \rightarrow f} = \int_0^{\infty} dt \langle f|i(t)\rangle \exp[i(E_0 + \epsilon_i)t] \exp(-\Gamma t), \quad (5)$$

where $|i(t)\rangle$ is the wavepacket after propagating on

the excited surface for a time t , Γ is the electronic dephasing rate, and ϵ_i is the energy of vibrational state $|i\rangle$. This expression has an intuitive interpretation. The system begins in the ground vibrational state $|i\rangle$, and at time $t=0$ the system interacts with the electronic transition operator to place it on the excited electronic surface. The wavepacket then evolves under the influence of the excited state Hamiltonian. The Raman amplitude is given by the half-Fourier transform of the overlap of the damped wavepacket at time t , $|i(t)\rangle$, with the final vibrational state $|f\rangle$. As resonance is approached, the dephasing rate decreases and the wavepacket evolves for longer times on the excited state surface, thereby developing overlap with new ground vibrational states. The appearance of overtones and new lines in the REP then provides information about the shape of the excited state surface along each vibrational coordinate.

Fig. 12a shows the common case of an excited-state potential energy surface whose minimum is displaced along some vibrational coordinate Q from the ground-state minimum. This could correspond to the stretching of a bond in the excited state. In the case of excitation into an unstable potential, the bond stretches and the molecule undergoes photofragmentation. The wavepacket picture envisions the Raman process as one in which the excitation light field produces a coherent superposition of ground and excited electronic states, i.e. an excited-state wavepacket,

which persists for the electronic dephasing time. As resonance is approached, the dephasing time increases, the wavepacket moves farther along the excited-state potential, and phase-coherent (i.e. Raman) emission into overtone levels is favored by increasingly large Franck–Condon factors. Thus as resonance is approached, the intensity of the fundamental line of Raman active modes increases while overtones of all modes along which excited-state nuclear motion occurs is enhanced.

In $M(\text{CO})_6$, the electronic transition which is approached is a formally forbidden g–g transition which appears with reasonable spectral intensity due to strong vibronic coupling. Fig. 12b and 12c show such a case. The potential energy minima of all stable g electronic states are not displaced along any nuclear coordinate, and unstable states have potential energy maxima which also are not displaced. A wavepacket on a stable g electronic potential energy surface broadens, and on an unstable g electronic surface splits into two pieces which move down both sides of the (two-dimensional projection of the) surface. Totally symmetric vibrational modes are Raman active and the intensities of fundamentals and all harmonics are enhanced as resonance is approached. Asymmetric modes are not allowed, but as resonance is approached the even overtones are enhanced. It is clear that odd overtones will not be enhanced since the Franck–Condon contributions from the two parts of

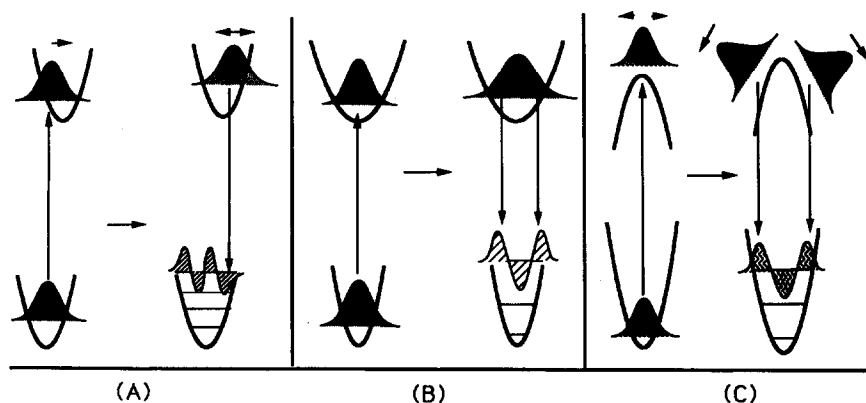


Fig. 12. (a) Schematic illustration of wavepacket evolution for a symmetric Raman active fundamental. As the wavepacket moves from its initial position it picks up overlap with overtone levels in the ground state. (b, c) Schematic illustration depicting wavepacket evolution for an asymmetric stretch in an excited state PES which is either stable (b) or unstable (c). As the wavepacket broadens or bifurcates it picks up overlap with even vibrational levels of the ground state.

the wavepacket will be out of phase. In the case of $\text{Cr}(\text{CO})_6$, we look for even overtones of asymmetric CO stretches since any likely reaction coordinate must involve such motions.

Fig. 13 shows RR data of $\text{Cr}(\text{CO})_6$ in methanol with both off-resonance (514 nm) and pre-resonance (351 nm) excitation wavelengths. The only Raman line between 100 and 600 cm^{-1} is the totally symmetric A_{1g} Cr–CO breathing mode. Since most of the Cr–CO asymmetric stretches (whose fundamentals do not appear in the Raman spectrum) are between 400 and 800 cm^{-1} [42], we must look at higher frequencies to observe overtones. Fig. 14 shows data from 1200– 1400 cm^{-1} . In the pre-resonant scan an additional new line is seen at 1332 cm^{-1} . This frequency corresponds to exactly twice the frequency of the ν_7 mode whose motion is shown in the fig. 14 inset. Very recent pulsed RR experiments [43] on $\text{Cr}(\text{CO})_6$ in cyclohexane do not reveal this overtone. These experiments show no asymmetric activity for excitation wavelengths within the ligand field transition band.

The ν_7 mode also has the correct symmetry to be the vibronic promoting mode. Only observation of higher overtones (which may require on-resonance excitation) will determine whether this coordinate

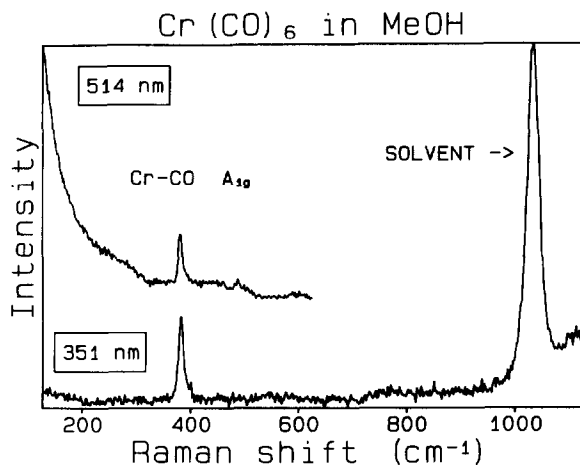


Fig. 13. Resonance Raman spectra of $\text{Cr}(\text{CO})_6$ in methanol in the spectral region $100\text{--}600\text{ cm}^{-1}$. The upper scan is for off-resonant 514 nm excitation while the lower spectrum is for pre-resonant 351 nm excitation. The only fundamental observed is the A_{1g} Cr–CO breathing mode which undergoes enhancement as resonance is approached.

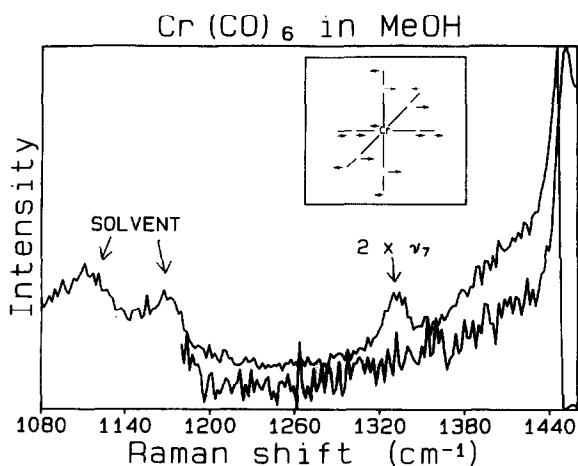


Fig. 14. Raman spectra of $\text{Cr}(\text{CO})_6$ in methanol for both off-resonant (lower trace) and pre-resonant (upper trace) excitation. Near resonance the second overtone of the ν_7 asymmetric stretch (shown in the inset) appears at 1332 cm^{-1} .

participates appreciably in the ligand ejection process or if the overtone appears primarily due to vibronic activity. Significant motion along the ν_7 coordinate during ligand ejection is certainly plausible; however, a more complete resonance excitation profile should be measured with a more versatile excitation source. We note that *ab initio* calculations of $\text{Cr}(\text{CO})_6$ potential energy surfaces are also under way [44].

Our examination of liquid-state organometallic photochemistry has included study of the bimetallic compounds $\text{M}_2(\text{CO})_{10}$, where $\text{M}=\text{Mn}$ or Re . Preliminary transient absorption data from $\text{Mn}_2(\text{CO})_{10}$ has been presented [13]. Excitation with ultraviolet light leads to either homolytic metal–metal ($\text{M}\text{--}\text{M}$) bond cleavage or CO loss. Clearly, an important part of the homolytic cleavage reaction coordinate is the metal–metal stretching coordinate. The symmetric $\text{M}\text{--}\text{M}$ stretching mode is strongly Raman active and should undergo strong resonance enhancement as described by the Albrecht A-term (eq. (2)) or by the wavepacket dynamics expression (eq. (5)). Resonance Raman spectra may indicate what other motions are involved, and most importantly could permit determination of the slope of the repulsive potential energy surface along which dissociation occurs. This information is crucial as input for molecular dynamics simulations or theoretical cal-

culations which could indicate the solvent role in M–M bond cleavage. Certainly solvent effects on the initial photochemical event should be stronger than in the case of $M(CO)_6$, since far more bulky and massive photofragments must move apart.

Fig. 15 shows preliminary resonance Raman spectra of $Mn_2(CO)_{10}$ in methanol. The on-resonance spectrum shows the fundamental and at least two overtones of the M–M stretching mode, and several combination bands involving the M–M stretch and an A_{1g} M–CO stretching mode [45]. These results will be discussed further in a subsequent publication. We present them here to illustrate the utility of resonance Raman spectra in conjunction with femtosecond time-resolved transient electronic absorption spectra of condensed-phase photochemical reactions. We are especially hopeful that this case may permit direct study of solvent effects on elementary bond breakage.

4. Summary

We have studied the photochemistry of $M(CO)_6$ in a variety of solvents. Short-time CO dissociation appears to be independent of the solvent implying that the dissociating fragment feels no significant force or

viscous drag from the solvent neighbors. The dissociation time does not change upon substituting tungsten or molybdenum for chromium, indicating that the triplet state does not play an essential role in the reaction. The dynamics of solvent complexation to the bare $M(CO)_5$ photofragment demonstrates that the solvent has no significant effect on which CO dissociates, and that the solvent undergoes no significant rearrangement before coordinating to the open site. Vibrational relaxation of the $M(CO)_5$ product occurs on the 50 ps time scale. Results from resonance Raman studies indicate that the ν_7 asymmetric M–CO stretch may be an important component of the most favorable reaction coordinate, but a more complete resonance excitation profile is needed. Resonance Raman spectra of $Mn_2(CO)_{10}$ were also presented and show extensive structure involving the metal–metal stretching mode along which photocleavage occurs.

Acknowledgements

This work was supported in part by NSF Grant No. CHE-8901722 and by contributions from DuPont, Perkin–Elmer, and the Alfred P. Sloan Foundation. Assistance by Dr. Mark Trulson in the acquisition and interpretation of Raman spectra is gratefully acknowledged.

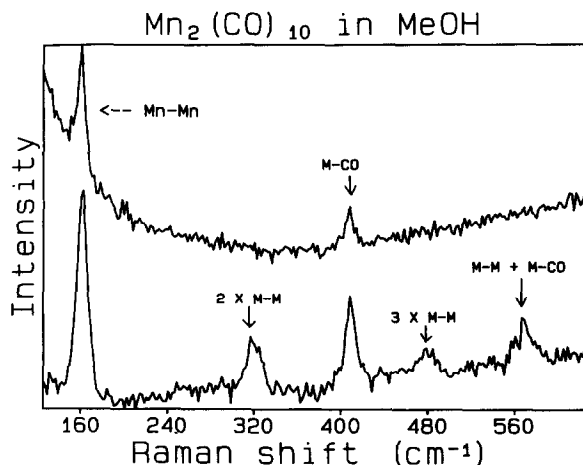


Fig. 15. Resonance Raman spectra of $Mn_2(CO)_{10}$ for both off-resonance (514 nm) and on resonance (351 nm) excitation. On resonance, the second and third overtones of the symmetric M–M stretch are enhanced as are combination bands between the M–M stretch and a symmetric M–CO stretch.

References

- [1] H.J. Foth, J.C. Polanyi and H.H. Telle, *J. Phys. Chem.* 86 (1982) 5027.
- [2] D. Imre, J.L. Kinsey, A. Sinha and J. Krenos, *J. Phys. Chem.* 88 (1984) 3956.
- [3] M. Dantos, M. Rosker and A.H. Zewail, *J. Chem. Phys.* 87 (1987) 2395.
- [4] M. Gruebele, G. Roberts, M. Dantos, R.M. Bowman and A.H. Zewail, *Chem. Phys. Letters* 166 (1990) 459.
- [5] S.A. Adelman and C.L. Brooks, *J. Phys. Chem.* 86 (1982) 1511.
- [6] S.H. Northrup and J.T. Hynes, *J. Chem. Phys.* 73 (1980) 2700.
- [7] B.M. Ladanyi and J.T. Hynes, *J. Am. Chem. Soc.* 108 (1986) 585.
- [8] A.G. Zawadzki and J.T. Hynes, *Chem. Phys. Letters* 113 (1985) 4761.
- [9] M.J. Rosker, F.W. Wise and C.L. Tang, *Phys. Rev. Letters* 57 (1987) 321.

- [10] J. Chesnoy and A. Mokhtari, *Phys. Rev. A* 58 (1988) 3566.
- [11] K.A. Nelson and L.R. Williams, *Phys. Rev. Letters* 58 (1987) 745.
- [12] A.G. Joly and K.A. Nelson, *J. Phys. Chem.* 93 (1989) 2876.
- [13] A.G. Joly and K.A. Nelson, in: *Advances in Laser Science IV* (AIP, New York) 333.
- [14] T.R. Fletcher and R.N. Rosenfeld, *J. Am. Chem. Soc.* 107 (1985) 2203.
- [15] J.D. Simon and X. Xie, *J. Phys. Chem.* 90 (1986) 6751.
- [16] L. Wang, X. Zhu and K.G. Spears, *J. Am. Chem. Soc.* 110 (1988) 8695.
- [17] M. Lee and C.B. Harris, *J. Am. Chem. Soc.* 111 (1989) 8963.
- [18] R.A. Seder, S.P. Church and E. Weitz, *J. Am. Chem. Soc.* 108 (1986) 4721.
- [19] D.P. Gerrity, L.J. Rothberg and V. Vaida, *J. Phys. Chem.* 87 (1983) 2222.
- [20] R.N. Perutz and J.J. Turner, *J. Am. Chem. Soc.* 97 (1975) 4791.
- [21] J.M. Kelly, C. Long and R. Bonneau, *J. Phys. Chem.* 87 (1983) 3344.
- [22] G.K. Yang, K.S. Peters and V. Vaida, *Chem. Phys. Letters* 124 (1986) 566.
- [23] J.K. Burdett, J.M. Grzybowski, R.N. Perutz, M. Poliakoff, J.J. Turner and R.F. Turner, *Inorg. Chem.* 17 (1978) 147.
- [24] S.-C. Yu, X. Xu, R. Lingle and J.B. Hopkins, in: *Ultrafast Phenomena VII*, eds. C.B. Harris, E.P. Ippen, G.A. Mourou and A.H. Zewail (Springer, Berlin, 1990), p. 434; *J. Am. Chem. Soc.*, in press.
- [25] S. Ruhman, B. Kohler, A.G. Joly and K.A. Nelson, *IEEE J. Quantum Electron.* QE-24 (1988) 470.
- [26] R. Mathies, A.R. Oseroff and L. Stryer, *Proc. Natl. Acad. Sci. USA* 73 (1976) 1.
- [27] R.H. Callender, A. Doukas, R. Crouch and K. Nakanishi, *Biochemistry* 15 (1976) 1621.
- [28] H.B. Gray and N.A. Beach, *J. Am. Chem. Soc.* 90 (1968) 5713.
- [29] A.L. Harris, M. Berg and C.B. Harris, *J. Chem. Phys.* 84 (1986) 788.
- [30] P.J. Hay, *J. Am. Chem. Soc.* 100 (1978) 2411.
- [31] N.A. Beach and H.B. Gray, *J. Am. Chem. Soc.* 90 (1968) 5713.
- [32] J. Nasielski and A. Colas, *Inorg. Chem.* 34 (1978) 1476.
- [33] J. Nasielski and A. Colas, *J. Organomet. Chem.*, 101 (1975) 215.
- [34] X. Xie and J.D. Simon, *J. Am. Chem. Soc.* 112 (1990) 1130.
- [35] S.Y. Lee and E.J. Heller, *J. Chem. Phys.* 71 (1979) 4777.
- [36] A.B. Myers and R.A. Mathies, in: *Biological Applications of Raman Spectroscopy* (Wiley-Interscience, New York, 1987, Chapter 2.
- [37] A.C. Albrecht, *J. Chem. Phys.* 34 (1961) 1476.
- [38] G.D. Korenowski, L.D. Ziegler and A.C. Albrecht, *J. Chem. Phys.* 68 (1978) 1248.
- [39] L.D. Ziegler and B. Hudson, *J. Chem. Phys.* 74 (1981) 982.
- [40] S.A. Asher and C.R. Johnson, *J. Phys. Chem.* 89 (1985) 1375.
- [41] R.R. Chadwick, D.P. Gerrity and B.S. Hudson, *Chem. Phys. Letters* 115 (1985) 24.
- [42] L.H. Jones, R.S. McDowell and M. Goldblatt, *Inorg. Chem.* 8 (1969) 2349.
- [43] D. Adelman and D.P. Gerrity, *J. Phys. Chem.* 94 (1990) 4055.
- [44] H. Sellers, A.G. Joly and K.A. Nelson, to be published.
- [45] D.M. Adams, M.A. Hooper and A. Squire, *J. Chem. Soc. A* (1971) 71.